Intermodal coupling of supermodes in a twin-core photonic crystal fiber and its application as a pressure sensor

Zhengyong Liu,[1,*] Ming-Leung Vincent Tse,[1] Chuang Wu,[2] Daru Chen,[3] Chao Lu,[2] and Hwa-Yaw Tam[1]

[1]*Photonics Research Center, Department of Electrical Engineering, The Hong Kong Polytechnic University, Hung Hom, Kowloon, Hong Kong*

[2]*Photonics Research Center, Department of Electronic and Information Engineering, The Hong Kong Polytechnic University, Hung Hom, Kowloon, Hong Kong*

[3]*Institute of Information Optics, Zhejiang Normal University, Jinhua 321004, China*

[*]*springlzy@gmail.com*

Abstract: In this paper, we experimentally demonstrated the fabrication and hydrostatic pressure characteristics of a twin-core photonic crystal fiber (TC-PCF). Mode couplings in the TC-PCF for *x*- and *y*-polarizations were analyzed simultaneously using group effective index of guiding modes. The output spectrum of the TC-PCF was modulated due to the combined couplings of the two polarizations. To the best of our knowledge, it is the first time to measure hydrostatic pressure through the dual-polarization mode coupling in a TC-PCF. The measured sensitivity of the pressure sensor was −21pm/MPa. The length of the TC-PCF used for pressure measurement was 20cm, which is much shorter than pressure sensor based on PM-PCF, and does not require any external polarizing components, meaning that it is a good candidate for compact pressure sensor.

OCIS codes: (060.5295) Photonic crystal fibers; (060.2280) Fiber design and fabrication; (060.2370) Fiber optics sensors; (280.5475) Pressure measurement.

References and links

1. P. Russell, "Photonic crystal fibers," Science **299**(5605), 358–362 (2003).
2. P. Russell, "Photonic-Crystal Fibers," J. Lightwave Technol. **24**(12), 4729–4749 (2006).
3. J. C. Knight, T. A. Birks, P. S. Russell, and D. M. Atkin, "All-silica single-mode optical fiber with photonic crystal cladding," Opt. Lett. **21**(19), 1547–1549 (1996).
4. T. A. Birks, J. C. Knight, and P. S. Russell, "Endlessly single-mode photonic crystal fiber," Opt. Lett. **22**(13), 961–963 (1997).
5. K. Saitoh, M. Koshiba, T. Hasegawa, and E. Sasaoka, "Chromatic dispersion control in photonic crystal fibers: application to ultra-flattened dispersion," Opt. Express **11**(8), 843–852 (2003).
6. A. Ortigosa-Blanch, J. C. Knight, W. J. Wadsworth, J. Arriaga, B. J. Mangan, T. A. Birks, and P. S. Russell, "Highly birefringent photonic crystal fibers," Opt. Lett. **25**(18), 1325–1327 (2000).
7. J. C. Knight and D. V. Skryabin, "Nonlinear waveguide optics and photonic crystal fibers," Opt. Express **15**(23), 15365–15376 (2007).
8. M. L. V. Tse, P. Horak, F. Poletti, N. G. Broderick, J. H. Price, J. R. Hayes, and D. J. Richardson, "Supercontinuum generation at 1.06 mum in holey fibers with dispersion flattened profiles," Opt. Express **14**(10), 4445–4451 (2006).
9. B. J. Mangan, J. C. Knight, T. A. Birks, P. S. J. Russell, and A. H. Greenaway, "Experimental study of dual-core photonic crystal fibre," Electron. Lett. **36**(16), 1358–1359 (2000).
10. Z. Wang, T. Taru, T. A. Birks, J. C. Knight, Y. Liu, and J. Du, "Coupling in dual-core photonic bandgap fibers: theory and experiment," Opt. Express **15**(8), 4795–4803 (2007).
11. W. Yuan, G. E. Town, and O. Bang, "Refractive index sensing in an all-solid twin-core photonic bandgap fiber," IEEE Sens. J. **10**(7), 1192–1199 (2010).
12. W. E. P. Padden, M. A. van Eijkelenborg, A. Argyros, and N. A. Issa, "Coupling in a twin-core microstructured polymer optical fiber," Appl. Phys. Lett. **84**(10), 1689–1691 (2004).
13. K. Saitoh, Y. Sato, and M. Koshiba, "Coupling characteristics of dual-core photonic crystal fiber couplers," Opt. Express **11**(24), 3188–3195 (2003).

#171939 - $15.00 USD Received 5 Jul 2012; revised 21 Aug 2012; accepted 29 Aug 2012; published 6 Sep 2012

14. J. R. Salgueiro and Y. S. Kivshar, "Nonlinear dual-core photonic crystal fiber couplers," Opt. Lett. **30**(14), 1858–1860 (2005).
15. B. Kim, T.-H. Kim, L. Cui, and Y. Chung, "Twin core photonic crystal fiber for in-line Mach-Zehnder interferometric sensing applications," Opt. Express **17**(18), 15502–15507 (2009).
16. M. K. Szczurowski, T. Martynkien, G. Statkiewicz-Barabach, W. Urbanczyk, and D. J. Webb, "Measurements of polarimetric sensitivity to hydrostatic pressure, strain and temperature in birefringent dual-core microstructured polymer fiber," Opt. Express **18**(12), 12076–12087 (2010).
17. M. Xu, L. Reekie, Y. Chow, and J. P. Dakin, "Optical in-fibre grating high pressure sensor," Electron. Lett. **29**(4), 398–399 (1993).
18. C. Wu, B.-O. Guan, Z. Wang, and X. Feng, "Characterization of Pressure Response of Bragg Gratings in Grapefruit Microstructured Fibers," J. Lightwave Technol. **28**(9), 1392–1397 (2010).
19. C. Wu, H. Y. Fu, K. K. Qureshi, B.-O. Guan, and H. Y. Tam, "High-pressure and high-temperature characteristics of a Fabry-Perot interferometer based on photonic crystal fiber," Opt. Lett. **36**(3), 412–414 (2011).
20. H. Y. Fu, C. Wu, M. L. V. Tse, L. Zhang, K. D. Cheng, H. Y. Tam, B. Guan, and C. Lu, "High pressure sensor based on photonic crystal fiber for downhole application," Appl. Opt. **49**, 2639–2643 (2010).
21. T. Chen, R. Chen, C. Jewart, B. Zhang, K. Cook, J. Canning, and K. P. Chen, "Regenerated gratings in air-hole microstructured fibers for high-temperature pressure sensing," Opt. Lett. **36**(18), 3542–3544 (2011).
22. D. Chen, G. Hu, and L. Chen, "Dual-core photonic crystal fiber for hydrostatic pressure sensing," IEEE Photon. Technol. Lett. **23**(24), 1851–1853 (2011).
23. M. Szpulak, T. Martynkien, and W. Urbanczyk, "Effects of hydrostatic pressure on phase and group modal birefringence in microstructured holey fibers," Appl. Opt. **43**(24), 4739–4744 (2004).
24. W.-P. Huang, "Coupled-mode theory for optical waveguides: an overview," J. Opt. Soc. Am. A **11**(3), 963–983 (1994).
25. M. L. V. Tse, H. Y. Tam, L. B. Fu, B. K. Thomas, L. Dong, C. Lu, and P. K. A. Wai, "Fusion splicing Holey fibers and single-mode fibers: A simple method to reduce loss and increase strength," IEEE Photon. Technol. Lett. **21**(3), 164–166 (2009).

1. Introduction

Photonic crystal fiber (PCF) is one kind of microstructured optical fiber that has an array of periodic air-holes in the cladding running along its length [1, 2]. Since the first single mode PCF was demonstrated [3, 4], the PCF technology has been found in many applications due to the specially tailored structures. It leads to the improvement of dispersion [5], birefringence [6], nonlinearity [7] of optical fibers, as well as supercontinuum generation [8]. Sensors that are based on PCFs also show promising results for measuring physical and biochemical parameters such as temperature, strain, pressure, refractive index, humidity, and chemical concentration. In particular, pressure sensor using optical fiber becomes quite significant and practical in various realms. Because of this, different designs of PCFs are needed and optimized to fulfill specific pressure application.

One special design of PCFs is twin-core photonic crystal fiber (TC-PCF) that has two solid cores separated by the centered air-hole. It has attracted much attention of researchers since its first demonstration [9]. It was reported that once the cores were separated at certain value (*e.g.* 15μm), the coupling between them became weaker. Theoretical and experimental analysis showed that this kind of coupling also occurred in twin-core photonic bandgap fiber (TC-PBGF), indicating that odd supermode has higher propagation constant [10]. This is very important for the refractive index sensors based on the coupling in TC-PBGF [11]. In a study of a twin-core microstructured polymer optical fiber, it was reported that the sensitivity of the coupling was strongly dependent on slight structural perturbations, such as the non-uniformity and the asymmetry of the holes [12].

One of the most important applications of TC-PCF is a mode coupler [13], with a short beat length of a few millimeters, a compact fiber based multiplexer/demultiplexer can be made. Moreover, nonlinear TC-PCF can support stable spatial optical solitons [14]. Due to the two cores in the center, Mach-Zehnder interferometer (MZI) can be implemented when the distance between two cores is large, because the mode coupling is weak and only slightly affects the light guidance in the two cores. It is utilized in some sensing realms. In 2007, Kim *et al* [15] demonstrated an in-line MZI based on TC-PCF and conducted strain, temperature and bending loss measurements, proving it a good candidate sensor with insensitivity to

#171939 - $15.00 USD Received 5 Jul 2012; revised 21 Aug 2012; accepted 29 Aug 2012; published 6 Sep 2012

bending. Similarly, the application is also found in polymer TC-PCF [16]. However, the later utilized the highly birefringence microstructured polymer optical fiber because of two large air-holes in the center, which certainly weakens the coupling between the cores.

In this work, the fabrication of a custom designed silica TC-PCF and the pressure responses of the fiber are reported. The two cores are so close (~2μm) that modes in each core will couple with each other strongly [13]. To our knowledge this is the first time for measuring hydrostatic pressure using silica TC-PCF based on mode couplings of x- and y-polarization. A pressure sensitivity of −21pm/MPa was obtained experimentally, which agreed well with the theoretical value of −19pm/MPa. It is higher than that of the pressure sensors based on normal FBGs (−3.04pm/MPa) [17], FBG in grapefruit microstructured fiber (−12.86pm/MPa) [18], or the PCF-based Fabry-Perot interferometer (−5.8pm/MPa) [19]. Fu *et al* reported a pressure sensor with high sensitivity of (3.24nm/MPa) at 1550nm using polarization-maintaining PCF (PM-PCF) based on the principle of Sagnac interference [20]. Nevertheless, longer fiber and additional 3-dB coupler should be used. Also, FBG was written on high birefringent microstructured fiber to measure the pressure by Chen *et al* in the year of 2011, with a sensitivity of 0.25pm/psi (36pm/MPa) [21]. The sensitivity for high birefringent PCF depends a lot on the principles used (*e. g.* Sagnac interference, FBG). Recently, Chen *et al* reported the feasibility of pressure sensing based on TC-PCF by simulation and obtained the sensitivity of −3.47pm/MPa [22]. However, they only considered the supermodes at x-polarization and ignored the group effective index of refraction, which is the key consideration when studying the transmission. The in-line fiber pressure sensor proposed here is simple to construct, repeatable and easy to handle.

2. Fabrication of TC-PCF

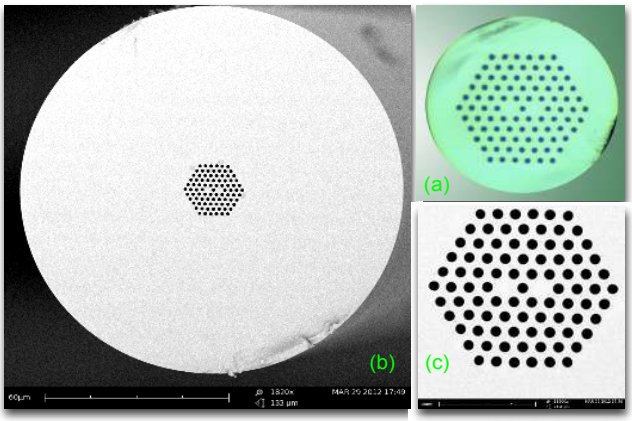

Fig. 1. (a) The microscope photo of the cross section of the cane and the SEM photos of the TC-PCF: (b) the whole fiber; (c) holes section

The two-core PCF was fabricated using the stack-and-draw method. Firstly, capillaries with diameter of 1.6mm were drawn from a tube (OD: 44mm, ID: 17.6mm) that has air fraction of 0.4. Then, the capillaries were stacked into a hexagonal structure. Two rods with the same diameter of capillaries were inserted and replaced two capillaries in the center, which will act as two cores eventually. The stacked preform was then drawn into canes with the diameter of 1.2mm (shown in Fig. 1(a)). One cane was chosen and inserted into a jacketing tube and finally drawn into fiber. The fiber drawing temperature was ~1900 ℃. During drawing, vacuum is needed to collapse the gaps between cane and jacketing tube. The SEM photos of the cross-section structure for the whole fiber and holes area are shown in Fig. 1(b) and Fig. 1(c). The outer diameter of the fiber is ~125μm and the cores diameter is ~2.5μm. The diameter of holes is ~1.1μm and the pitch of the structure is ~1.85μm, thus the air fraction is

#171939 - $15.00 USD Received 5 Jul 2012; revised 21 Aug 2012; accepted 29 Aug 2012; published 6 Sep 2012

0.59. The air fraction in the fiber is a little larger than that of the original tube due to the expansion of the structured cane during fiber drawing. The fiber loss of the TC-PCF measured at 1550nm was ~4.4dB/m. The loss was acceptable for sensing.

3. Mode coupling of dual polarizations in the TC-PCF

The TC-PCF formed with triangular lattice of circular holes has two missing holes in the center, which act as two cores along the fiber. These two cores become two independent waveguides with mode coupling. The beat length increases with increasing of the distance between two cores [13]. In other words, the mode coupling is stronger when the cores are closer. We used a commercial COMSOL© software to do the simulation and calculated the modes with full-vector finite element method. The parameters of TC-PCF used in the simulation were the same as those of fabricated fiber, with hole diameter d = 1.1μm and the pitch Λ = 1.85μm. The refractive index of silica was 1.444 and the refractive index of air was 1.

According to the investigation, there are two supermodes (even and odd mode) for each polarization. Thus, we obtained x-polarized even mode, x-polarized odd mode, y-polarized even mode and y-polarized odd mode (shown in Fig. 2(a)). When the operating wavelength is 1550nm, the phase effective indices of each mode are: $n_{p,x\text{-}even}$ = 1.4003668, $n_{p,x\text{-}odd}$ = 1.3993208, $n_{p,y\text{-}even}$ = 1.4002832, $n_{p,y\text{-}odd}$ = 1.3993959, respectively. It should be noted that the effective index of even mode is larger than that of odd mode, which is opposite in the TC-PBGF [10]. Thus, the phase modal birefringence is $B_{x,p} = |n_{p,x\text{-}even} - n_{p,x\text{-}odd}| = 1.046 \times 10^{-3}$ for x-polarization and $B_{y,p} = |n_{p,y\text{-}even} - n_{p,y\text{-}odd}| = 8.873 \times 10^{-4}$ for y-polarization. Figure 2(a) illustrates the relationship of phase effective index of refraction and wavelength for each supermode. It is easy to see that the phase effective refractive index decreases with increasing wavelength.

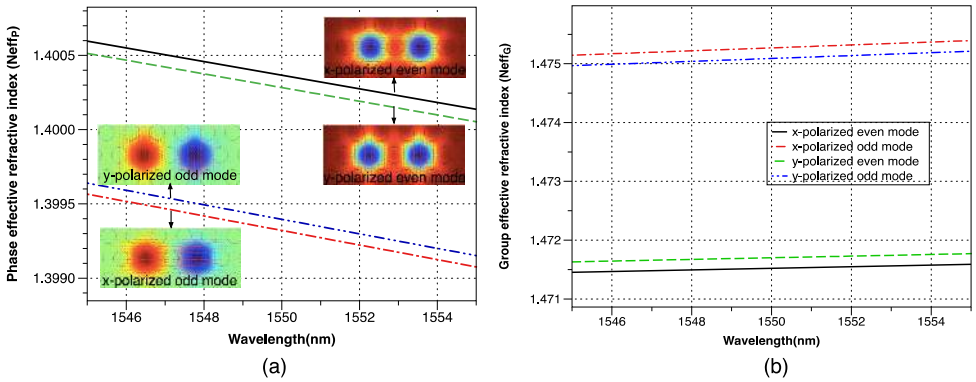

Fig. 2. The phase effective index of refraction (a) and the group effective index of refraction (b) as the function of wavelength. The insets of (a) are the electric field profiles of x-polarized even mode, x-polarized odd mode, y-polarized even mode, and y-polarized odd mode.

The group effective index of refraction n_g is dependent on phase effective index n_p and wavelength. The dependence can be expressed by

$$n_g = n_p - \lambda \frac{dn_p}{d\lambda}. \quad (1)$$

To obtain n_g and the differentiation accurately in Eq. (1), the relationship between n_p and λ, shown in Fig. 2(a), is numerically approximated with a sixth-degree polynomial. This approximation has been used in [16, 23] for the same purpose.

#171939 - $15.00 USD Received 5 Jul 2012; revised 21 Aug 2012; accepted 29 Aug 2012; published 6 Sep 2012

Figure 2(b) shows the calculated relationship of group effective index of refraction as a function of wavelength for the four supermodes individually. The group effective index of odd mode is larger than that of even mode, which is opposite to the phase effective index. Moreover, it increases with wavelength, which is also different from phase effective index. The group modal birefringence is $B_{x,g} = |n_{g,x\text{-}even} - n_{g,x\text{-}odd}| = 3.745 \times 10^{-3}$ at the wavelength of 1550nm. In terms of y-polarization, it is $B_{y,g} = |n_{g,y\text{-}even} - n_{g,y\text{-}odd}| = 3.386 \times 10^{-3}$. This implies that, as for transmission, group effective index instead of phase effective index should be considered in the TC-PCF.

The distance between two cores of the TC-PCF we fabricated is ~2μm, which strengthens the coupling in the TC-PCF. The coupling length for *x*-polarization is given by the expression

$$L_c(\lambda) = \frac{\lambda}{2\,|\,n_{g,x\text{-}even} - n_{g,x\text{-}odd}\,|} = \frac{\lambda}{2\Delta n_{x,group}}, \tag{2}$$

where $n_{g,x\text{-}even}$, $n_{g,x\text{-}odd}$ represents the group effective index of *x*-polarized even and odd mode respectively, while $\Delta n_{x,group}$ stands for their difference. The coupling coefficient eventually changes with the surrounding pressure due to the relationship between coupling length and effective index. In terms of *x*-polarization, the optical power transferred from one core to the other in a TC-PCF with a length of *L* can be formulated as [24]

$$|\ (\lambda) = \sin^2(\frac{\pi}{2L_c}L) = \sin^2(\frac{\pi}{\lambda}\Delta n_{x,group}L). \tag{3}$$

It is worth noting that x-polarization and y-polarization exist in the TC-PCF simultaneously, which means that the total intensity of light should involve both of them at the output. Due to *x*-polarization and *y*-polarization are orthogonal, the total intensity at the output can be

$$I = I_1 + I_2. \tag{4}$$

By substituting Eq. (3) into Eq. (4), the total intensity can be expressed by

$$|\ (\lambda) = 1 - \cos[\frac{\pi}{\lambda}(\Delta n_{x,group} + \Delta n_{y,group})L].\cos[\frac{\pi}{\lambda}(\Delta n_{x,group} - \Delta n_{y,group})L]. \tag{5}$$

It can be predicted that the spectrum at the output is modulated. For the fringe spacing, if considering small range of wavelength, it can be approximated as

$$\Delta\lambda = \frac{2\lambda^2}{(\Delta n_{x,group} + \Delta n_{y,group})\cdot L}. \tag{6}$$

Figure 3 shows the experimental spectrum of the 110-cm-long TC-PCF, as an example, using the setup shown in the inset. A piece of the TC-PCF mentioned above with a length of 110cm was used and manually spliced to SMFs at both ends using the technique described in [25]. A Furukawa FITEL-177 fusion splicer was used. The main parameters of arc power, arc duration time are set to 2 steps and 200ms. During splicing, a broadband source (BBS) centered at 1550nm and an Optical Spectrum Analyzer (OSA) were utilized to monitor the transmission spectrum. The position of TC-PCF was manually adjusted along the x- and y-axis. Initially, the two fibers were aligned roughly center-to-center, and weak interference pattern was observed, indicating weak coupling within the TC-PCF. An offset in the alignment was then introduced to obtain higher fringe contrast. Further adjustments in the x-y position of the fibers were made until the highest fringe contrast was obtained. At that point, the core of SMF was assumed to be aligned with one of the cores of TC-PCF, and the fibers were fused together by arc discharges. The combined splicing loss was ~3dB. Obviously, the whole spectrum is modulated due to the combination of the coupling of even and odd modes

#171939 - $15.00 USD Received 5 Jul 2012; revised 21 Aug 2012; accepted 29 Aug 2012; published 6 Sep 2012

at both polarizations. The fringe spacing measured is ~0.676nm, which is quite close to the calculated value (~0.613nm) using Eq. (6).

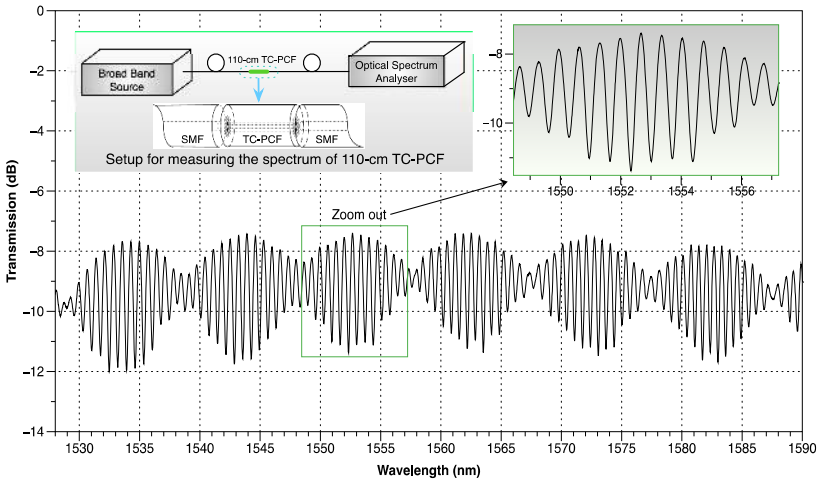

Fig. 3. The experimental spectrum of 110-cm-long TC-PCF at the output measured using OSA with a resolution of 0.02nm. The upper left inset is the setup utilized.

4. Hydrostatic pressure characteristics of TC-PCF

When the TC-PCF subject to hydrostatic pressure, the anisotropic stress results in the geometrical deformation, which leads to the variation of the refractive index of fused silica due to the photoelastic effect. This relationship can be concluded as

$$\begin{aligned} n_x &= n_0 - C_1\sigma_x - C_2(\sigma_y + \sigma_z) \\ n_y &= n_0 - C_1\sigma_y - C_2(\sigma_x + \sigma_z), \end{aligned} \tag{7}$$

where n_0, n_x, n_y represent the refractive indexes of fused silica without pressure and refractive index of fused silica at x-polarization and y-polarization after pressure applied. σ_x, σ_y and σ_x are the stress components and the stress-optic coefficient of silica, C_1, C_2 are $6.5 \times 10^{-13}\text{m}^2/\text{N}$, $4.2 \times 10^{-12}\text{m}^2/\text{N}$ respectively. Consequently, the pressure loaded can change the coupling in TC-PCF, which is manifested by affecting the difference of phase effective index of refraction and finally the difference of group effective index of refraction in Eq. (5). Since this influence on refractive index is linear because of photoelastic effect, the transmission spectrum of TC-PCF shifts linearly with pressure applied as expected.

Figure 4 illustrates the setup used to measure the hydrostatic pressure. A piece of the TC-PCF with a length of 20cm was spliced to SMFs using the same method described above. The fabricated sensor was then put into a hydrostatic pressure chamber with a maximum pressure of 45 MPa. The applied pressure can be calibrated through a pressure gauge (CONST 211) linked with the chamber. The pressure gauge has the resolution of 0.001MPa. A broadband source centered at 1550nm was used and an Optical Spectrum Analyzer (OSA, YOKOGAWA AQ6370) with a resolution of 0.02nm was utilized to measure the transmission spectrum.

#171939 - $15.00 USD Received 5 Jul 2012; revised 21 Aug 2012; accepted 29 Aug 2012; published 6 Sep 2012

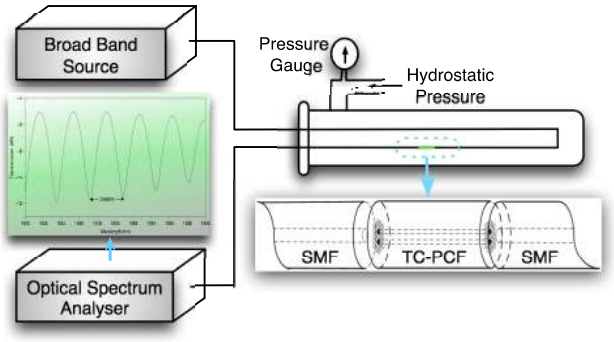

Fig. 4. Schematic diagram of the setup for hydrostatic pressure measurement, the left inset illustrates the transmission spectrum of 20-cm-long TC-PCF with the fringe spacing of 3.688nm

In the experiment, the pressure increased with a step of 5MPa. Figure 5(a) shows the spectrum shift after the hydrostatic pressure was applied from 0MPa to 45MPa. Figure 5(b) enunciates the wavelength at one minima as functions of the hydrostatic pressure. The sensitivity is −21pm/MPa, with high linearly fitting of $R^2 = 0.996$. The same experiment was repeated, and the result of second measurement (red square) was well agreed with the result of the first measurement (black circle). This indicates that the TC-PCF pressure sensor has high repeatability, which is extremely important in practical use. Due to resolution limit of 0.02nm of optical spectrum analyzer, the smallest pressure of 1MPa can be measured and calibrated for the given OSA. This pressure sensitivity is acceptable for highly pressure (>100MPa) measurement, giving ~1% accuracy, which is comparable to some commercial pressure sensors (*e.g.* ~2% accuracy from FISO Technologies Inc.). Moreover, the resolution can also be improved on the condition of using an OSA with higher resolution.

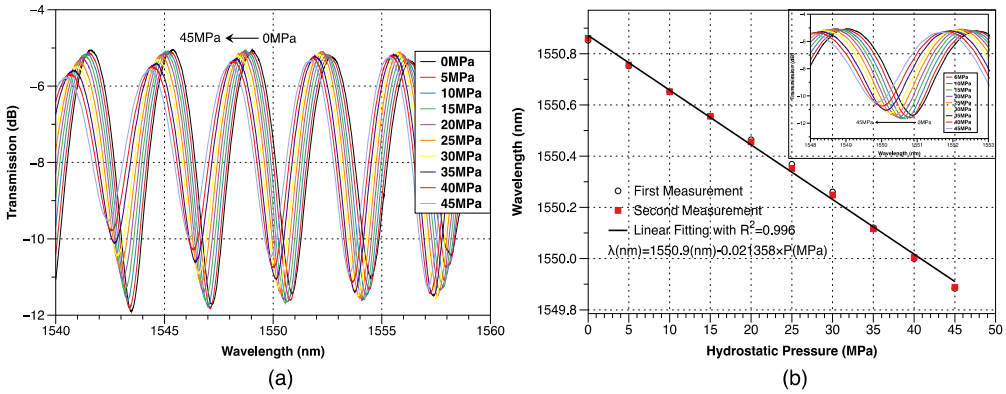

Fig. 5. (a) Transmission spectrum shift of the sensor with the hydrostatic pressure changing from 0MPa to 45MPa. (b) Wavelength shift at one minima as functions of hydrostatic pressure applied, the top-right inset shows the shift of spectrum around the minima

The response of hydrostatic pressure was also simulated using COMSOL© in order to compare with experimental sensitivity. The same structure of TC-PCF was used with the hole diameter d = 1.1μm and the pitch Λ = 1.85μm, which make the simulation close to experiment as much as possible. Firstly, the phase effective index of refraction at different wavelength was calculated accurately through COMSOL©. Then, the same calculation was conducted to obtain the phase effective index of refraction after pressure applied from 0MPa to 45MPa. During calculation, RF Module and Plane Stress Module in Multiphysics were

#171939 - $15.00 USD Received 5 Jul 2012; revised 21 Aug 2012; accepted 29 Aug 2012; published 6 Sep 2012

utilized. After that, group effective index of refraction was computed through Eq. (1), which helps to get the spectrum at different pressure eventually. Figure 6 manifests the comparison of the simulation (black line) and experimental (blue dashed line) response of pressure. As shown in the figure, the simulation sensitivity of pressure is −19pm/MPa, which is quite close to the experimental value −21pm/MPa. The experimental sensitivity is a little larger than that in simulation because the structure in the real fiber is not ideal. It is inevitable that the diameter of holes and the pitch cannot always be the same during fabrication even if the defect is quite small.

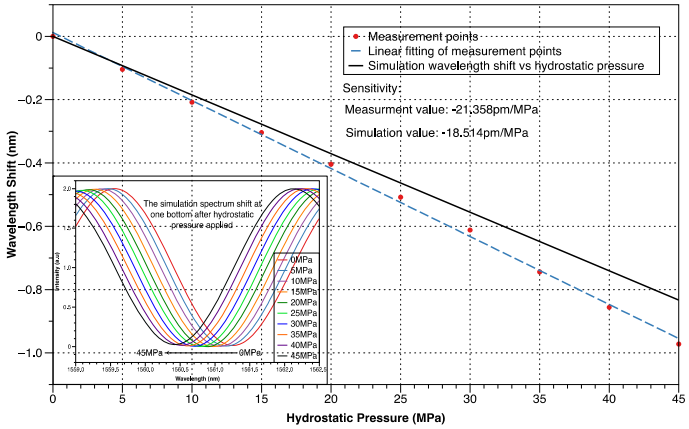

Fig. 6. The simulation and experimental wavelength shift as functions of hydrostatic pressure.The simulation spectrum shift at one minima is shown in the left-bottom inset

Moreover, it should be noted that the fringe spacing obtained in simulation using coupling theory is ~3.44nm (shown in the inset of Fig. 6), which is fairly close to the experimental value of 3.688nm. This further verifies the coupling occurring in the TC-PCF. In addition, during measurement, the intensity of the detected dip increases slightly with the increasing of pressure applied. This is because the whole spectrum is modulated (see Fig. 3), which means specific minima can be suitable for pressure measurement. However, since the length of TC-PCF is short (*e.g.* 20cm), the modulation period is large enough and does not affect the pressure measurement result.

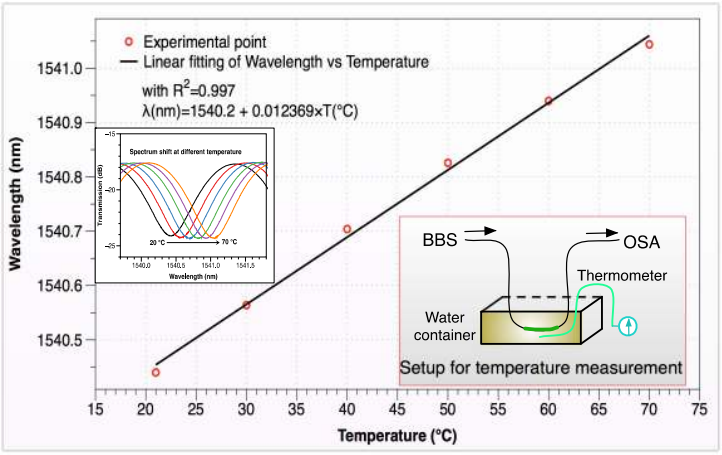

Fig. 7. The temperature response of the TC-PCF sensor, the spectra shift at different temperature and the setup used are showing in the insets.

#171939 - $15.00 USD Received 5 Jul 2012; revised 21 Aug 2012; accepted 29 Aug 2012; published 6 Sep 2012

The temperature response for this sensor has also been measured in the experiment. The results are illustrated in Fig. 7. The same BBS and OSA were used to launch the light and detect the output. 20cm TC-PCF sensor was put in a water container, which was heated from 20þC to 70þC with a step of 10þC. The experimental results were linearly fitted with R^2 = 0.997. Hence, a sensitivity of 12.4pm/þC to the temperature is obtained. As a sensor, even though it has a little cross-sensitivity, the thermal response can be easily compensated by fiber Bragg grating method, which means the cross-sensitivity will affect the practical use very little.

5. Conclusion

We fabricated a silica TC-PCF using the stack-and-draw method. This kind of TC-PCF was designed and drawn with small distance between the two cores, which strengthen the mode coupling in the TC-PCF. By following simulation, the phase effective index of refraction of even mode was found larger than that of the odd mode for both *x*- and *y*-polarization. It is different from the reported TC-PBGF. Moreover, calculations show that the group effective index of refraction of even mode in TC-PCF is smaller than that of the odd mode. The large difference between phase and group index in the TC-PCF indicates that the latter one should be considered in terms of transmission. The experimental spectra of 110cm and 20cm of TC-PCF further verified the mode couplings considering *x*- and *y*-polarization simultaneously. And the transmission spectrum is modulated. Finally, hydrostatic pressure characteristics are numerically and experimentally investigated from 0MPa to 45MPa, giving the sensitivity of −19pm/MPa and −21pm/MPa individually. The sensitivity is higher than normal FBG, FBG in PCF, and FPI sensor based on PCF. The length of the TC-PCF used for pressure measurement was 20cm, which is much shorter than the existing PM-PCF-based pressure sensor, indicating that it is a good candidate for compact pressure sensor.

Acknowledgments

This paper is supported by the Central Research Grant of The Hong Kong Polytechnic University under the Postdoctoral Fellowship (Project No. G-YX2D), Project G-U746 and Projects of Zhejiang Province (No. 2011C21038 and No. 2010R50007).

#171939 - $15.00 USD Received 5 Jul 2012; revised 21 Aug 2012; accepted 29 Aug 2012; published 6 Sep 2012